Available online at www.sciencedirect.com
ScienceDirect
Journal of the European Ceramic Society 29 (2009) 757–762
www.elsevier.com/locate/jeurceramsoc

Evaluation of 316 L porous stainless steel for SOFC support

S. Molin [a], M. Gazda [b], B. Kusz [b], P. Jasinski [a,*]

[a] *Faculty of Electronics, Telecommunications and Informatics, Gdansk University of Technology, ul. Narutowicza 11/12, 80-952 Gdansk, Poland*
[b] *Faculty of Applied Physics and Mathematics, Gdansk University of Technology, ul. Narutowicza 11/12, 80-952 Gdansk, Poland*

Received 29 April 2008; received in revised form 14 July 2008; accepted 17 July 2008
Available online 28 August 2008

Abstract

Solid oxide fuel cells (SOFCs) supported on porous steel substrates are recently gaining much attention, because fabrication cost of SOFC might be significantly reduced. In this paper high temperature properties of porous stainless steel 316 L for application in SOFCs are evaluated. The 316 L was investigated using thermogravimetric analysis, XRD analysis and electrical measurements of scales formed on steel surface. The YSZ ceramic electrolyte was deposited on the 316 L and interaction of formed interlayer was evaluated. The results show that the 316 L is applicable only for SOFCs operated below 500 °C.

Keywords: Corrosion; Fuel cells; Electrical properties; ZrO_2

1. Introduction

The stainless steel has been considered mainly for use as a dense interconnector/bipolar plate between anodes and cathodes.[1] The application of the stainless steel in fuel cell has several advantages over ceramic materials. This is related to their high thermal conductivity, high electrical conductivity and ease of manufacturing. Also the price of steel, which is about an order of magnitude lower than the price of ceramic materials, is an important factor. When dense steels are used, still thick ceramic supporting layers need to be employed for fabrication of SOFC. However, incorporation of porous steel provides an opportunity to the use of much thinner ceramic layers and thus leads to further reduction of costs. The porous steel has similar advantages as the dense one and can well serve as a mechanical framework for SOFCs. There is a limited number of steel powders suitable for fabrication of metallic porous supports. Yet, a ferritic steel 70Fe30Cr,[2,3] 430 L,[4] Crofer 22 APU[5,6] and austenitic HastelloyX[7] were tested as possible candidates for porous SOFC supports. The ferritic steels are more suitable as they have thermal expansion coefficient, which is comparable to that of fuel cell ceramics ($\sim$10 ppm K^{-1}). On the other hand, austenitic stainless steel has a high thermal expansion coefficient ($\sim$16 ppm K^{-1}) but it is in general more suitable for work in high temperatures. In the metallic SOFC support the high level of porosity is required and therefore very high specific surface area of steel is exposed to air. This leads to the excessive oxidation of porous steel at elevated temperatures and this problem has to be solved before widespread application of steel.

In this work a porous, austenitic 316 L stainless steel is evaluated. Steel was obtained from Mott Corporation, USA. This is a steel with high chromium (16–18.5%) and nickel (10–14%) content and with additions of molybdenum (2–3%), manganese (<2%) and silicon (<1%). Its relatively high thermal expansion coefficient ($\sim$16 ppm K^{-1} for dense steel) indicates that for successful use with ceramics a low temperature deposition method should be used to minimize mechanical stresses. In this paper, the porous 316 L was used to deposit the electrolyte layer ($Zr_{0.84}Y_{0.16}O_{2-x}$) directly onto metallic substrate by low temperature method. Obtained in this way electrolyte/metallic structure can be used to form SOFC by infiltration into porous metallic structure of appropriate metalo-organic precursor solutions in a similar manner as described by Tucker et al.[8] For example Ni nitrate solution can be used to prepare anode, while La,Sr,Mn nitrates to form LSM cathode.

2. Experimental

Porosity of samples was measured by Archimedes method using kerosene as a medium. X-ray diffraction was performed

* Corresponding author. Tel.: +48 58 3471323; fax: +48 58 3471757.
E-mail addresses: pijas@eti.pg.gda.pl, pijas@biomed.eti.pg.gda.pl (P. Jasinski).

0955-2219/$ – see front matter © 2008 Elsevier Ltd. All rights reserved.
doi:10.1016/j.jeurceramsoc.2008.07.027

using the Philips X'Pert diffractometer with Cu Kα radiation. Sample surfaces were measured at room temperature. The ICDD PDF database was used for qualitative phase identification and description. The FEI-Philips XL30 ESEM scanning electron microscope equipped with the EDAX Sapphire energy dispersion analysis system was used for collecting images and elemental mappings, respectively. The accelerating voltage of 15 kV was used. The elements of oxygen, zirconium, yttrium, chromium and iron were taken into consideration.

Electrical conductivity of steel samples was measured in a four-terminal configuration using bar-shaped sample (Fig. 1a) of 0.7 cm in width and 4 cm in length between voltage probes. The current and voltage contacts were made from gold wires attached by gold paste (ESL 8880, USA). A constant current of 1 A was maintained during measurement of voltage drop by the Keithley 2400 SourceMeter.

Electrical conductivity of oxide scale formed on steel surface was carried out using a sandwich type setup presented in Fig. 1b. Platinum contacts (ESL 5542, USA) were brush painted on opposite facets and fired at 750 °C for 30 min to ensure proper bonding to the substrate. Samples were placed in a measurement rig in a tube furnace and two platinum wires were attached to each contact to enable 4-point conductivity measurement. Constant current density of 70 mA cm^{-2} was flowing through the sample and voltage drop was measured. For these measurements the Keithley 2400 SourceMeter was used. The obtained resistance was corrected for the area of contacts and divided by a factor of two to obtain an area specific resistance (ASR) of one side of the scale formed on steel.

Cyclic thermogravimetry measurements were conducted by placing a sample in a furnace at a desired temperature for a specific amount of time. The temperatures of 400 °C and 800 °C were chosen. The former is the maximum ceramic layer deposition temperature, to which a sample is exposed for decomposition of an organic residue. The latter is the working temperature of a typical intermediate temperature SOFCs. The heating and cooling rate of 260 °C/h was used. After each oxidation time mass of a sample was measured on a microbalance and the sample were placed back into the furnace. Only the time at soak temperature is taken into account. The rate of high temperature oxidation is usually limited by the diffusion of cations from the bulk of the steel to its surface. In this case the oxidation can be described by a parabolic rate law:

$$\left(\frac{\Delta m}{A}\right)^2 = k_p t \quad (1)$$

where Δm, mass change due to oxidation, A, area of the sample subjected to oxidation, k_p, parabolic rate law constant, and t, time of oxidation.

In case of the porous samples it is hard to determine the surface area subjected to oxidation, therefore a modified law is used:

$$\left(\frac{\Delta m}{m_0}\right)^2 = k_p t \quad (2)$$

where m_0 is the initial mass of the sample.

Samples subjected to the thermogravimetric measurements as well as specially oxidized samples were used for XRD measurements to evaluate phase formation at different oxidation temperatures and times.

Ceramic yttria stabilized zirconia (YSZ) electrolyte was deposited by a Net-shape technology. It is comprised of a combined colloidal suspension and polymer precursor method. Details of ceramic membrane preparation are described in Refs. 9,10. This is a low temperature ceramic processing method that can result in fully dense electrolyte layers with maximum processing temperature not exceeding 1000 °C.

3. Results and discussion

A SEM image of the as received 316 L porous substrate is presented in Fig. 2. The pores of approximately 50 μm in diameter and grain size of about 20 μm can be seen. High porosity of the support enables easy gas flow through the channels. However this surface, which is relatively rough, can provide difficulties for deposition of continuous thin ceramic films.

Results of cyclic oxidization of 316 L in air and humidified hydrogen are shown in Fig. 3. The oxidation at 400 °C in hydrogen does not cause visible scale formation. In air only minor oxidation can be measured and after ~100 h it ceases. At 800 °C

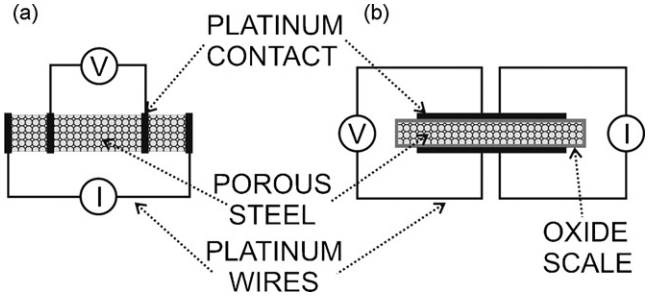

Fig. 1. Electrical conductivity measurement setups for assessment of conductivity of steel (a) and oxide scale (b).

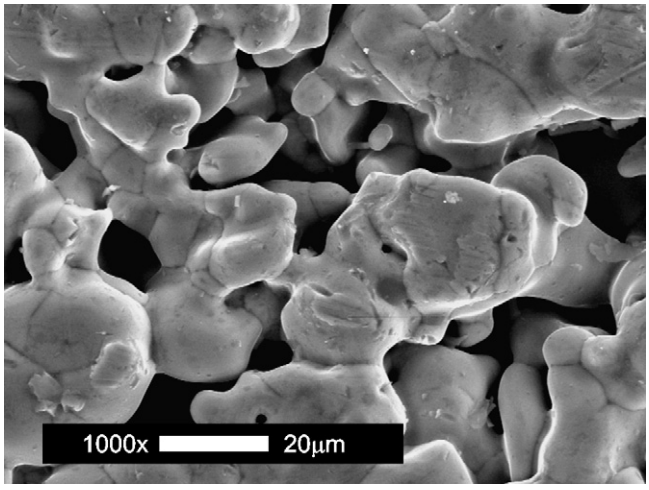

Fig. 2. SEM surface image of the as obtained porous 316 L steel sheet.

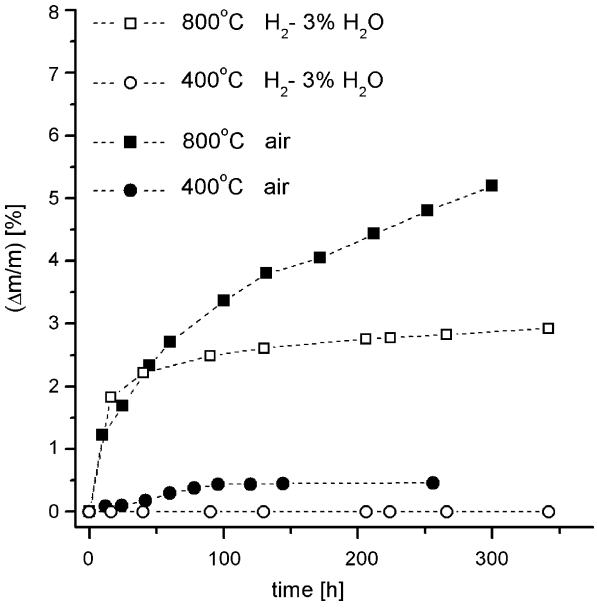

Fig. 3. Results of the thermogravimetric analysis of 316 L stainless steel in air and humidified hydrogen at 400 °C and 800 °C.

both in hydrogen and air the oxide scale grows rapidly. The oxidation rate in air is faster than in hydrogen. The initial rate up to about 50 h is similar but after this time in the hydrogen the rate of scale growth is slowed down. This can be related to different scale compositions in those atmospheres what will be described later on in the text. After 300 h of oxidation in air the sample has gained 5% of its initial mass. In hydrogen the change is 3%. These are too high values to consider 316 L as a supporting material operating at 800 °C. However, spallation of oxide scale has not occurred in either case, which is an advantage. This can be related to small amount of silicon (<1 wt.%) in steel that is known for scale adherence improvement.

XRD spectra of samples oxidized in air at different temperatures for 65 h are shown in Fig. 4. In all the cases the reflexes can be attributed to the steel substrate (either γ or γ and α phases) and oxides like Cr_2O_3 and Fe_2O_3. However the Cr_2O_3–Fe_2O_3 phase diagram shows that these oxides form solid solution in the temperature range examined here[11] so this phase is written in general form as a $(Fe,Cr)_2O_3$. The reflexes corresponding to the oxides are hardly visible at 500 °C but they tend to increase at higher temperatures. The Rietveld analysis indicates that at 500 °C and 700 °C the Fe_2O_3 dominates in the scale. At higher temperatures both the Cr_2O_3 and Fe_2O_3 oxides are present in similar amounts. For comparison, the spectra of the as received steel are also shown. The process of quite fast oxidation of the 316 L steel at temperature above 500 °C may be caused by its sensitization to the intergranular corrosion.[12] It proceeds by forming the chromium depleted regions which results in deterioration of the protective Cr_2O_3 layer. As a result a breakaway oxidation begins. The ferrite formation in austenitic steel after high temperature treatment was confirmed elsewhere as well.[13] Therefore 700 °C seems to be the upper limit of operation for this steel because, as mentioned before, the electrical conductivity is stable up to this temperature and XRD is showing steady rate of

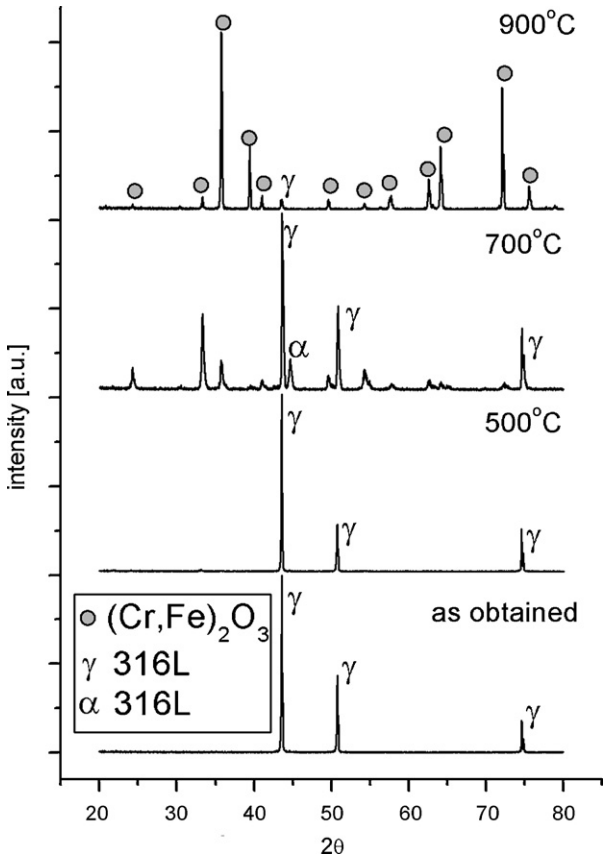

Fig. 4. XRD spectra after 65 h of oxidation in air at different temperatures. For comparison a spectra of as obtained sample is shown.

scale formation. At 900 °C this steel is subjected to rapid and severe corrosion that can be noticed on XRD spectra and also during optical examination of the sample.

XRD spectra (not shown here) of samples annealed in humidified hydrogen at different temperatures showed only chromium oxide scale. It is also indicated by green sample color in comparison to dark grey/black after oxidation in air. As was mentioned earlier this can be the cause of different rate of oxide scale growth.

The electrical conductivity measurements of 316 L steel are presented in Fig. 5. The conductivity levels remained stable even for long dwell times at temperatures below 700 °C. Also thermal cycling did not change the conductivity. At 800 °C a quasi monotonic decrease of conductivity in time was observed (not shown here). However the changes were not severe and tended to stabilize in time. Conductivity of the steel was measured prior to the heat treatment (while heating to 800 °C) and after oxidation at 800 °C for 300 h. Both results are presented in Fig. 5. Before and after oxidation steel shows metallic type and level of conductivity. It should be noted that when measuring steel in a sandwich-like configuration, shown in Fig. 1b, the conductivity of the oxidized sample is a few orders of magnitude lower than that of the not-oxidized one. It suggests that the oxide scale determinates the resistance. The ASR should remain as low as possible for SOFCs application. The acceptable ASR limit is considered to be 100 mΩ cm^2 after 40,000 h of SOFC

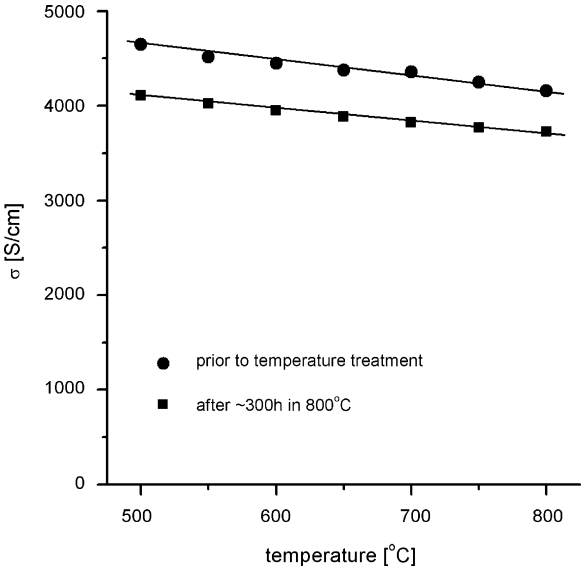

Fig. 5. Conductivity of a porous 316 L steel bar as a function of temperature without and with heat treatment for about 300 h at 800 °C.

operation.[14] The ASR of porous 316 L as a function of time at 800 °C is shown in Fig. 6. A rapid resistance growth is seen and only after 200 h the ASR exceeds the limit value. Two different slopes of ASR time dependence can be seen in Fig. 6. The oxidation rate up to about 150 h is lower than that above 150 h (1.1 mΩ cm^2 h^{-1}). This different behavior can be related to change of oxide scale composition. It is also possible that due to the sample porosity and surface roughness the oxide grows unevenly, what influences contact area with platinum paste.

SEM image of ceramic YSZ electrolyte deposited on porous substrate is shown in Fig. 7. The image shows a sample with maximum processing temperature of 400 °C. The average thickness can be estimated to be 15 μm. The roughness of porous support is very well covered and the surface of formed layer is smooth

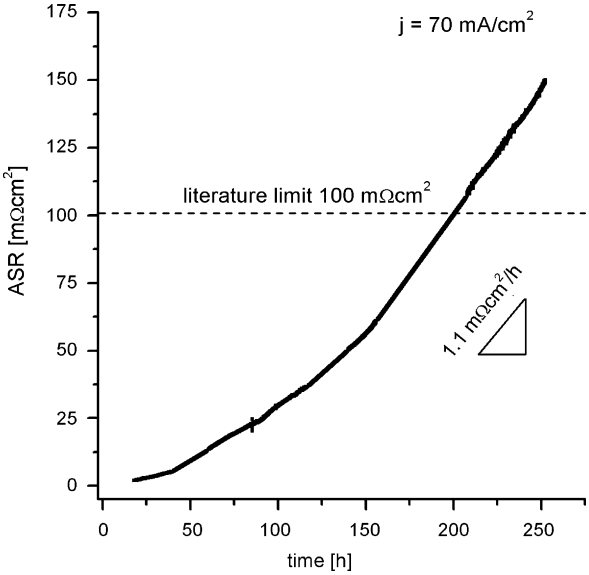

Fig. 6. Area specific resistance of oxide scale formed on porous 316 L steel measured in air at 800 °C.

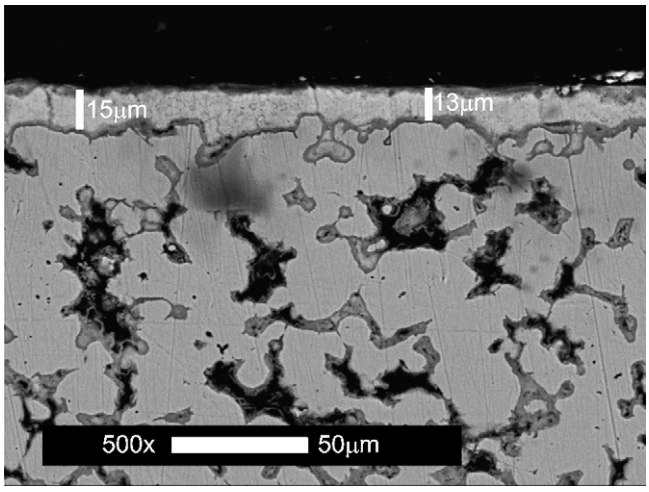

Fig. 7. SEM image of 316 L steel with deposited ceramic YSZ layer.

and continuous. The electrolyte penetrates inside the pores even 100 μm below the surface of the steel. This is related to the deposition method comprised of a polymer impregnation step. This issue is rather advantageous because it improves adherence of deposited layer and the surface area available for electrochemical reaction. Between the deposited ceramic membrane and the steel substrate a continuous intermediate layer is visible. It is an oxide scale that formed during repeated heating up to 400 °C in air atmosphere. This corresponds to thermogravimetric results in which some mass gain was reported. However it seems that the oxide scale is thicker close to the surface than inside the bulk of the steel.

The XRD spectra of the deposited ceramics after different heat treatment cycles are presented in Fig. 8. The spectra of as deposited and annealed at 600 °C and 800 °C were collected. In

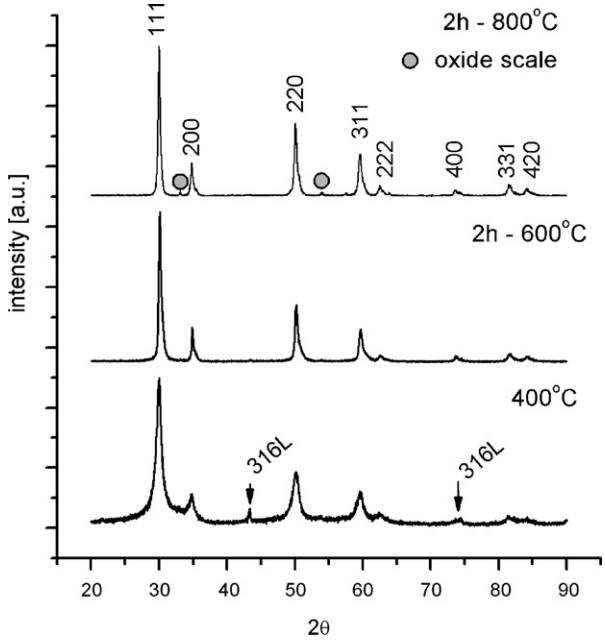

Fig. 8. XRD spectra of a ceramic YSZ layer deposited on 316 L steel substrate after different processing temperatures.

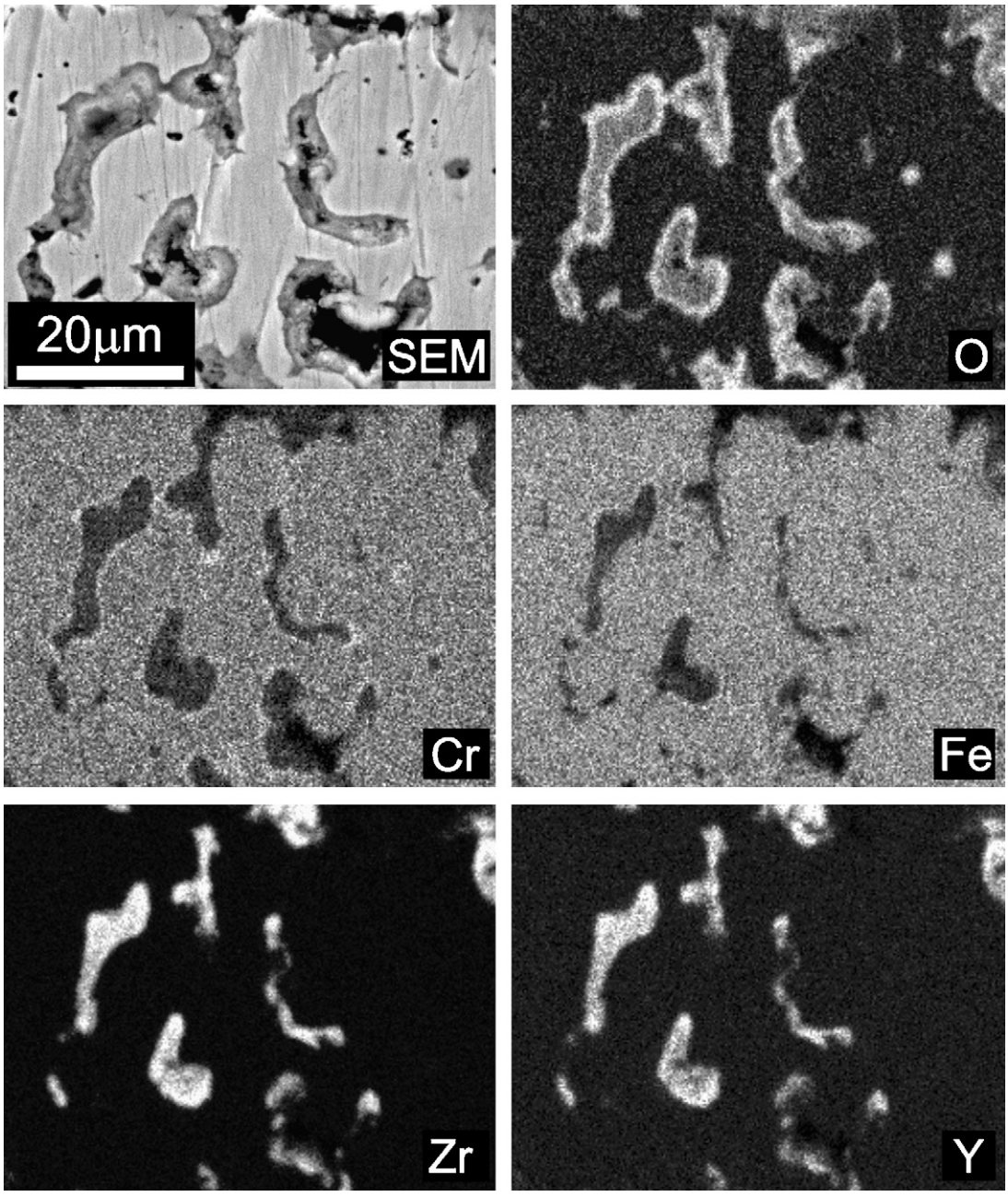

Fig. 9. Elemental mapping of 316 L steel support of a area just beneath the deposited ceramic layer.

case of the sample with the maximum processing temperature of 400 °C the XRD reflexes corresponding to the YSZ and the steel substrate are visible. This is due to small thickness of not fully crystallized ceramic layer. After annealing at 600 °C only the ceramic layer is visible. Further increasing the temperature to 800 °C causes the excessive oxide growth beneath the ceramics, so that it becomes visible in the spectra. The sharp peaks of YSZ are still present while these of the oxide are very small. The oxide scale can be identified as $(Fe,Cr)_2O_3$ as described earlier.

For additional evaluation of the composition of oxide scale formed on the steel beneath the YSZ surface the EDX elemental mapping was performed and presented in Fig. 9. The area scanned just below the deposited electrolyte was chosen for evaluation. The scanned area consists of the steel and the pores impregnated with the YSZ electrolyte. This infiltration can be confirmed in zirconium (Zr) and yttrium (Y) elemental mapping images. In this areas more oxygen is detected as well (image of O mapping). However, the oxygen level is even higher at the interface between YSZ and steel (in oxide scale). When comparing images of iron (Fe) and chromium (Cr) mapping it can be noticed that the oxide scale is also rich in iron. This indicates that the oxide scale is mainly composed of Fe_2O_3.

4. Conclusions

The oxidation behavior and electrical conductivity of porous 316 L stainless steel were evaluated in this paper. The oxidation investigation showed high oxidation rate due to extended

surface area subjected to corrosive atmospheres. Oxidation in air and humidified hydrogen follows modified Wagner law. The oxide scale was found to be a $(Fe,Cr)_2O_3$ for oxidation in air and Cr_2O_3 for oxidation in humidified hydrogen atmosphere, as evaluated by XRD analysis. That was further confirmed by EDX mapping, which proved that the oxide scale formed in air contained mainly Fe_2O_3. Electrical conductivities of steel and oxide scale were measured at 800 °C. Oxide scale conductivity, that is governed mainly by presence of iron oxide phase, is not sufficient to provide a suitable support for SOFC. The 316 L reaches the ASR limit of 100 $m\Omega\,cm^2$ just after 200 h of annealing. The presented results demonstrate that 316 L is an inappropriate SOFC support material at the temperatures higher than 500 °C, in which the oxidation process in air is severe.

Acknowledgement

This work is supported by the project MNiSW 3 T10B 077 29.

References

1. Singhal, S. C. and Kendall, K., *High Temperature Solid Oxide Fuel Cells*. Elsevier, The Netherlands, 2003.
2. Antepara, I., Villarreal, I., Rodriguez-Martinez, L. M., Lecanda, N., Castro, U. and Laresgoiti, A., Evaluation of ferritic steels for use as interconnects and porous metal supports in IT-SOFCs. *J. Power Sources*, 2005, **151**, 103–107.
3. Matus, Y. B., De Jonghe, L. C., Jacobson, C. P. and Visco, S. J., Evaluation of ferritic steels for use as interconnects and porous metal supports in IT-SOFCs. *Solid State Ionics*, 2005, **176**, 443–449.
4. Hui, S., Yang, D., Wang, Z., Yick,. S., Deces-Petit, C., Qu, W., Tuck, A., Maric, R. and Ghosh, D., Metal-supported solid oxide fuel cell operated at 400–600 °C. *J. Power Sources*, 2007, **167**, 336–339.
5. Stöver a, D., Hathiramani, D., Vaßen, R. and Damani, R. J., Plasma sprayed components for SOFC applications. *Surf. Coat. Technol.*, 2006, **201**, 2002–2005.
6. Vaßen, R., Hathiramani, D., Mertens, J., Haanappel, V. A. C. and Vinke, I. C., Manufacturing of high performance solid oxide fuel cells (SOFCs) with atmospheric plasma spraying (APS). *Surf. Coat. Technol.*, 2007, **202**, 499–508.
7. Huang, Q.-A., Oberste-Berghaus, J., Yang, D., Yick, S., Wang, Z., Wang, B. and Hui, R., Polarization analysis for metal-supported SOFCs from different fabrication processes. *J. Power Sources*, 2008, **177**, 339–347.
8. Tucker, M. C., Lau, G. Y., Jacobson, C. P., DeJonghe, L. C. and Visco, S. J., Performance of metal-supported SOFCs with infiltrated electrodes. *J. Power Sources*, 2007, **171**, 477–482.
9. Anderson, H. U., Nasrallah, M. M. and Chen, C. -C., Method of coating a substrate with a metal oxide film from an aqueous solution comprising a metal cation and a polimerizable organic solvent. US Patent 5,494,700.
10. Suzuki, T., Jasinski, P., Petrovsky, V., Anderson, H. U. and Zhou, X. -D., Method for electrode deposition for solid oxide fuel cells. US Patent, US 2006/0280861 A1.
11. Qu, W., Jian, L., Ivey, D. G. and Hill, J. M., Yttrium, cobalt and yttrium/cobalt oxide coatings on ferritic stainless steels for SOFC interconnects. *J. Power Sources*, 2006, **157**, 335–350.
12. Baccalaro, M., Mattern, A., Hauer, I., Pohl, M., Schneider, G. and Flaig, A., How to resist the stress of temperature. *Met. Powder Rep.*, 2006, **6**, 18–22.
13. Bautista, A., Velasco, F., Campos, M., Rabanal, M. E. and Torralba, J. M., Oxidation behavior at 900 °C of austenitic, ferritic, and duplex stainless steels manufactured by powder metallurgy. *Oxid. Met.*, 2003, **59**, 373–393.
14. Fergus, J. W., Metallic interconnects for solid oxide fuel cells. *Mater. Sci. Eng. A*, 2005, **397**, 271–283.